Journal of Alloys and Compounds 609 (2014) 215–221

Contents lists available at ScienceDirect

Journal of Alloys and Compounds

journal homepage: www.elsevier.com/locate/jalcom

Effect of grain size reduction of AA2124 aluminum alloy powder compacted by spark plasma sintering

A. Eldesouky [a], M. Johnsson [b], H. Svengren [b], M.M. Attallah [c], H.G. Salem [d,*]

[a] Department of Materials Science and Engineering, Egypt Japan University of Science and Technology, Alexandria, Egypt
[b] Department of Materials and Environmental Chemistry, Stockholm University, Stockholm, Sweden
[c] IRC in Materials Processing School of Metallurgy & Materials, University of Birmingham, Edgbaston, United Kingdom
[d] Mechanical Engineering Department, American University in Cairo, Cairo, Egypt

ARTICLE INFO

Article history:
Received 14 February 2014
Received in revised form 31 March 2014
Accepted 19 April 2014
Available online 26 April 2014

Keywords:
AA2124
Nano-powder
Mechanical milling
Spark plasma sintering

ABSTRACT

Nanocrystalline (Average grain size ~200 nm) bulk AA2124 alloy was produced through high energy ball milling of microcrystalline powder followed by spark plasma sintering (SPS) at 480 °C with a holding time of 10 min. The effect of initial particle and grain size on the microstructural evolution as well as on the relative density and mechanical properties of the specimens consolidated through SPS and hot pressing (HP) at the same temperature for 60 min was investigated for ball milled nano-powders (NP), as well as as-received micro-powders (MP). Results showed that the NP specimens consolidated with SPS had the highest microhardness values compared to the other specimens despite not achieving full densification. On the other hand, a general increase in density, hardness, and compressive strength was observed for all SPS consolidates compared to HP. The presence of aluminum oxide and its influence on the consolidation process as well as the resulting mechanical properties of the bulk specimens is also discussed.

1. Introduction

Over the last few decades, there has been an ever increasing interest in nanocrystalline (NC) materials due to their extremely high strength and hardness [1,2], high diffusion rates [3], high fatigue resistance [4], corrosion resistance [3] and improved tribological properties [5] compared to conventional microstructured materials. Most researchers recently categorize materials into 3 main groups based on their grain size: NC materials (<100 nm), ultrafine grain materials (100 nm–1 μm) and microcrystalline (MC) materials (>1 μm) [4]. Several techniques have been used recently for the synthesis of NC structures such as inert gas condensation (vapor phase), electro-deposition and rapid solidification (liquid phase) and mechanical attrition or ball milling (solid state). Ball milling has been utilized since the late 1980s to synthesize NC solid state powder materials using relatively low cost and simple equipment [6]. The consolidation of the NC powders to bulk solids with full/near full density takes place through one of various sintering routes such as the conventional hot pressing (HP) [7,8], hot isostatic pressing (HIP) [9,10] and more recently spark plasma sintering (SPS) [11,12]. SPS has evident superiority over other conventional sintering techniques due to the higher heating rates, lower sintering temperatures and much shorter holding times required for full/ near full density consolidation, this in turn leads to enhanced materials characteristics especially in the sintering of NC materials as little time is allowed for grain growth, which is a major concern when it comes to synthesis of NC bulk products.

AA2124 is a wrought Al–Mg–Cu alloy that is broadly used in industrial applications that require high strength and fracture toughness at elevated temperatures [7]. AA2124 is often named the aircraft alloy because of its extensive applications in the aerospace industry. The utilization of powder metallurgy techniques has contributed to the enhancement of mechanical properties of the AA2124 alloy. Salem and Sadek [8] successfully produced nano sized particles of AA2124 powder by high energy ball milling of 40 μm initial particle size powder. The mechanical behavior of the consolidated bulk NC AA2124 produced from MC and NC powders through HP followed by equal channel angular processing was also investigated. Results showed that the NC powder (that have previously gone through high energy ball milling) was strain hardened and was only consolidated at higher temperatures (480 °C and prolonged holding times between 60 and 90 min), while specimens processed at lower sintering temperatures lacked integrity. However, the combination of high temperature and long holding

* Corresponding author. Tel.: +20 1222186290; fax: +20 27957565.
E-mail addresses: ahmed.eldesouky@gmail.com (A. Eldesouky), mats.johnsson@mmk.su.se (M. Johnsson), henrik.svengren@mmk.su.se (H. Svengren), m.m.attallah@bham.ac.uk (M.M. Attallah), hgsalem@aucegypt.edu (H.G. Salem).

http://dx.doi.org/10.1016/j.jallcom.2014.04.136
0925-8388/

time resulted in coarsening of the initial NC structure, which in turn led to a loss in the mechanical properties.

SPS has been utilized in several studies to retain the nanostructure of aluminum alloy powders during consolidation. Ye et al. investigated the effect of processing of cryomilled Al 5083 powder via SPS [13]. X-ray Diffraction (XRD) grain size calculations before and after SPS showed that the average grain size of the alloy only increased from 25 nm to 50 nm (from powder to bulk state). Subsequently, the hardness values obtained through nanoindentation for specimens of AA5083 produced via SPS were highly improved in comparison to conventional sintering methods were grain coarsening takes place on a larger scale. In another study the combination of cryomilling and SPS of AA-5356/B4C nanocomposites powder was found to largely improve the microhardness and flexural strengths of the bulk nanocomposite. Rana et al. [14] investigated the effect of SPS on mechanically milled AA6061 (Al–Mg–Si) micro-alloy powder. The average grain size after 20 h of milling was ~35 nm and increased to only ~85 nm after processing with SPS at 500 °C. Microhardness and compressive tests were carried out on the consolidated near full density specimens of both unmilled and milled powders and the results showed significant increase in both hardness and compressive strengths for the milled nanocrystalline powders as a result of the very fine grain size.

The present work examines the effect of high energy ball milling on the processing and properties of AA2124 powder. Microstructural evolution and mechanical properties of the spark plasma sintered specimens were studied and compared to results obtained from hot pressing of the same set of powders from the previous study by Salem and Sadek [8]. The discrepancy in phase formation and its subsequent effect on the mechanical properties and the microstructure for both set of powders under each processing condition is also discussed.

2. Processing and experimental procedures

Gas atomized AA 2124 powder (composition: Al–3.9 Cu–1.5 Mg–0.65 Si–0.1) with an average particle size of 40 μm and 87 nm average grain size (supplied by the Aluminium Powder Company APC Ltd.) was used in this study. The powder was ball milled using a FRITCH high energy ball mill for 36 h at a speed of 500 RPM, with a ball-to-powder ratio of 30:1 to produce the nanocrystalline powders. The resulting powder was characterized using Field Emission Scanning Electron Microscope (FESEM) to ascertain the conditions of the nanocrystalline structure prior to processing. A 15 mm diameter die was used in the SPS setup (which is the same die diameter used in the previous study using HP) for both unmilled micro-powders (which will be referred to as MP) and milled nano-powders (which will be referred to as NP). A heating rate of 100 °C/min up to 400 °C followed by a 40 °C/min up to 480 °C was employed for the SPS experiment followed by holding time of 10 min under a pressure of 60 MPa. While a significantly lower heating rate (16 °C/min up to 480 °C) was used in the previous HP experiment followed by a holding time of 30 min under a pressure of 624 MPa. Fig. 1 shows a comparative diagram for the heating cycles for both HP and SPS experiments. The densities of the sintered compacts were then measured using Mettler Toledo XS 205 digital densitometer in xylene solution after cleaning the specimens from the thin graphite layer that was formed at the die/specimen interface.

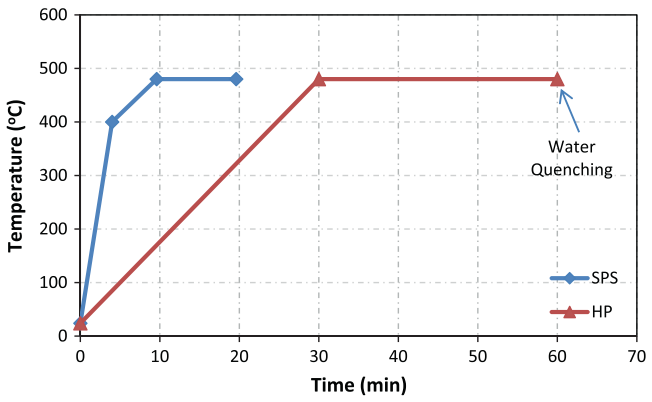

Fig. 1. SPS and HP heating cycles.

Micro-hardness was performed using a Mitutoyo VHN 810 micro indenter at 100 g and 15 s dwell time. Compression tests were conducted under 50 KN in a MTS Universal testing machine at a cross-head speed of 0.5 mm/min. Microstructural evolution of the powders and sintered specimens were investigated using a Leica optical microscope, and LEO SUPRA 55 FESEM. Higher magnification imaging of the sintered powders as well as dispersoids identification was conducted using JEOL 2010 TEM operated at 200 kV with a spatial resolution of 1.9 Angstrom. Grain size measurements were conducted using a Diano Co. X-ray diffractometer (Cu Kα, $\lambda = 0.1542$ nm), to assess the grain growth (via Scherrer's formula for peak broadening) of the NC powder compared to the as-received MC powder under the various SPS conditions. Background subtraction and calculation of full width at half maximum were done through the diffractometer associated software. Microstructural evolution and mechanical properties of all SPS samples were compared to conventional HP reported in [8].

3. Results and discussion

FESEM imaging of the powders before and after milling revealed that the high energy of milling imposed on the powder during the 36 h milling time led to the refinement of the micron-powders (45 μm average particle size and 87 nm average grain size) down to ultrafine feathery shaped nanoscale powder (<100 nm in size that were agglomerated in clusters ranging between 2 and 30 μm in size with average substructure size of ~20 nm) (Fig. 2). Fig. 3a shows the XRD peaks at $2\theta = 44$ for powders milled from 0 to 60 h. Obvious peak broadening and intensity decline can be seen with the increase in milling time which is evidence of internal grain size reduction. During the mechanical milling process, the milling balls impact the powder particles causing them to plastically deform and subsequently work harden, which is then followed by fracture and re-welding of the particles. In a previous study, increasing the MT to 6 h resulted in a significant refinement of the crystallite size from an average of 78-to-32 nm as shown in Fig. 3(b). Further milling resulted in a gradual refinement in the crystallite size to a minimum of 15.6 nm at 36 h of milling time. Increasing the MT above 36 h did not result into further structural refinement. The observed slight increase in crystallite size up to 17.7 nm although insignificant could be due to the heat generated during the long period of MT up to 60 h, which may result into coarsening of the nanoscale structure. Milling beyond 60 h is necessary to trace the structural behavior with increasing MT [7].

Density measurements were carried on both MC and NC specimens processed via SPS and compared to the previous results of HP. Table 1 summarizes the relative densities, hardness and compressive properties produced. It can be seen from the density values that near full densities were achieved for the MC specimens (where no ball milling has taken place) under both SPS and HP conditions. On the other hand, the NC specimens only reached a final relative density of ~95.5% and 93% of theoretical for both SPS and HP, respectively. This result might initially contradict with basic concepts in sintering as smaller size particles are expected to sinter faster due to shorter diffusion distances, increased number of contact points and increased surface area, and high surface area energetic particles [15]. However, the presence of oxide thin films on aluminum based powder particles is known to hinder the sintering process [16]. The presence of oxide thin layer has been confirmed using EDX analysis in the previous work by Salem and Sadek [8] where it was also shown that fragmentation of the oxide layer occurs under applied pressure for as received powders, this will open up metal-to-metal contact points, which explains the full densification of the MP. On the other hand, the severely strain hardened NP produced through high energy ball milling will be less likely to deform under the applied pressure in HP or SPS and therefore the oxide layer will continue to act as a barrier to the sintering process. Moreover, the densities of the NP and MP

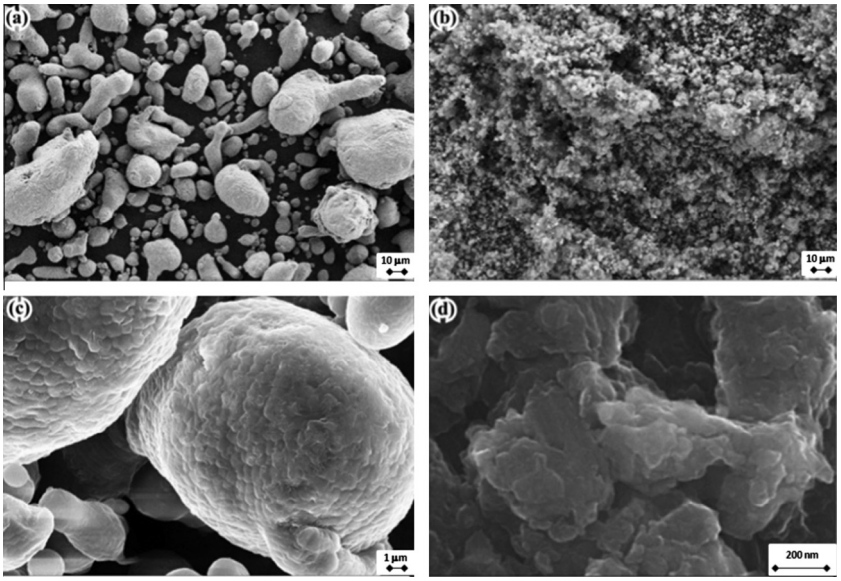

Fig. 2. FESEM images for the AA2124 un-milled powder (a, c) and after 36 h of milling (b, d).

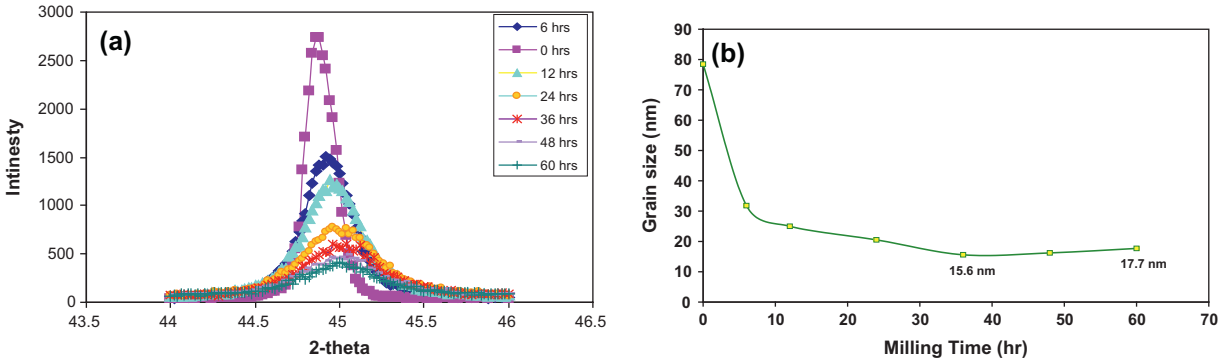

Fig. 3. (a) XRD diffraction pattern showing the peak broadening at $2\theta = 44^{\circ}$ and (b) grain size variation as a function of milling time.

Table 1
Physical and mechanical properties of specimens consolidated through SPS and HP. Each data point represents the average and range of 5 readings per data point.

Powder condition	Relative density (%)	Microhardness (VHN)	Compressive yield strength (MPa)
MP-SPS	99.4 ± 0.22	155.5 ± 1.3	300 ± 2.2
NP-SPS	95.5 ± 0.6	250.2 ± 0.9	703 ± 3.6
MP-HP	99.2 ± 0.4	97.5 ± 3.4	226 ± 5.4
NP-HP	93 ± 1.3	181.6 ± 5	590 ± 4.8

produced via SPS showed slightly higher improvement in densification than those produced through HP, regardless of the significantly shorter sintering time at 480 °C used for SPS.

In spite of the lower final densities achieved in the NP specimens, there was a significant increase in the microhardness values (compared to the MP specimens) regardless of the sintering technique, this is mainly due to the inherent properties of nanostructured powders following the Hall–Petch relation as well as the excessive strain hardening induced by 36 h of ball milling. Furthermore, the increased presence of surface oxides in nano-powders due to their high surface area to volume ratio will also contribute to the enhanced hardness of the sintered material.

A comparison of the hardness values (based on 5-measurement per sample) of SPS products to HP products shows that significantly higher microhardness levels were reached with SPS (for the same initial powder size specimens) due to the faster heating rate and much shorter holding time at the sintering temperature (10 min holding time in SPS compared to 60 min in HP) which does not allow ample time for grain coarsening. Furthermore, new phase formation might occur during SPS of, which could also contribute to the hardness and compressive yield strength enhancement. Such phenomenon was reported by several researchers for various Al-alloys processed via SPS where newly formed nanostructured phases (50–100 nm) are developed during sintering [14,17].

Fig. 4 shows the compressive offset yield stress–strain curves for NP and MP specimens processed via SPS and HP. In general, specimens processed via SPS showed higher compressive yield strength compared to HP specimens as a result of the improved material properties due to the higher heating rates and shorter sintering duration. The MP consolidated powders via SPS should showed high ductility (did not fracture under compression, Fig 4b) almost 2× that of the HP consolidates and higher yield strength almost 1.3× higher. Similar observations were made for the NP. Consolidated NP specimens possessed via SPS showed significant increase in both compressive yield strength and ductility by 1.2× and 2.5× that of the HP counterparts. However, the displayed decrease in ductility of the NP compared to the MP consolidated specimens can be explained by the incompressibility of the compacted heavily strain hardened particles (induced by BM) which

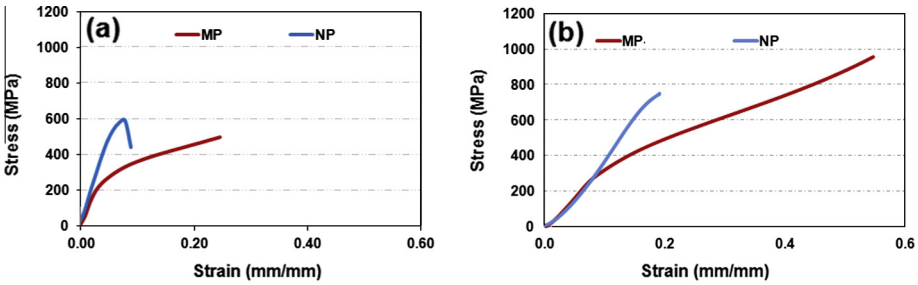

Fig. 4. Compressive stress–strain curves of (a) specimens processed through HP and (b) specimens processed with SPS.

was sustained by the measured relatively lower density levels achieved (~93.5%) compared to the near fully dense MP specimen (~99.4%). The relative softness of the Sintered of the as received MP allows the compressibility under pressure resulting in the closer of the voids along the particles boundaries and along triple points and hence enhancement of the atomic diffusion along the particle surfaces. On the other hand, the incompressibility of the strain hardened NP particles promoted the formation of micro-voids along the boundaries and at triple points, which explains the low relative measured densities produced compared to the MP (Table 1). Furthermore, both powder configurations processed with SPS showed enhanced ductility over hot pressed specimens.

In addition, the tendency for formation of encapsulating oxide layers (explained earlier in this paper) in smaller sized particles might have also contributed to the exacerbated strength as these layers do not only hinder the densification, but also forms a barrier to metal/metal bonding between particles, which would certainly affect the overall mechanical properties of the consolidate. Lack of metal/metal bonding produced micro-voids at triple junctions, which could have induced local stress concentration points resulting in premature failure under compressive loading, which will be revealed by OM investigation.

Microstructural analysis using optical microscopy for MP specimens showed that the SPS products had a higher degree of uniform diffusion along the particle boundaries (Fig. 5). High magnification images also showed finer grain structures in the SPS specimens compared to HP specimens. Clear formation of dark particles was observed at triple points for both specimens, which was identified as Al_2O_3 based particles in a previous research conducted on sintered Al 5083 alloy powder [13]. TEM images (Fig. 6) of the SPS specimens show the evolution of well-defined and mostly relaxed grains with average grain size (AGS) ~1.4 μm. A lath like phase aligned perpendicular to [0 1 1] and [0 0 1] directions and rod like (31–50 nm size) precipitates were also identified in the structure with base centered orthorhombic lattice. Further phase analysis using d-space measurements also revealed the presence of coarse Mn-rich dispersoids with a tetragonal structure about 214 nm long and 110 nm in width.

Investigation of the NP consolidated specimens via SPS and HP confirmed higher porosity content compared to MP specimens but with a much finer structure (Fig. 7), which explains the displayed decrease in ductility compared to the SPS sintered MP. The oxide dark particles observed along the boundaries and triple points in the MP consolidates (Fig. 5c and d) via SPS and HC, respectively are observed within the delineated heavily deformed Al 2124 matrices shown in Fig. 7c and d, respectively. It is clear that samples processed via SPS (Fig. 7c) shows heavily deformed structure compared to a more relaxed structure using conventional HC (Fig. 8d). It is anticipated that the influence of milling on the morphology of the Al_2O_3 particle morphology and distribution has a significant influence on the produced mechanical properties post sintering.

Fig. 8 shows TEM images for the NP consolidates where an obvious refinement of the structure can be observed compared to the MP specimens (Fig. 6). AGS of ~200 and ~380 nm were measured for the NP consolidates sintered via SPS and HP, respectively, compared to AGS of 1.4 μm and 2.2 μm for MP consolidates sintered via SPS and HP, respectively. It is clear that the SPS process was incapable of relaxing the heavily delineated (Fig. 8a) structure, which had a strong influence on the significant increase in microhardness and compressive yield strength. On the other hand, the longer sintering time associated with HP resulted in a relatively relaxed structure and relatively coarser structure (Fig. 8b).

Investigation of the fracture behavior of the consolidated MP and NP powders via SPS and HC provides an explanation of the displayed mechanical properties. Scanning electron micrographs of the HC fracture surface of the MP specimens after the compression tests shows evidence for antiparticle fracture (Fig. 9). This morphology is a consequence of an embrittlement in the particle bonds, which was not expected for the ductile micro-powders of AA21214. However, this result is in line with the previous conclusion dealing with the presence of fragmented oxide films at the interface between particles. Fig. 9b shows the fragmented oxide films (circled) along the consolidated particle boundaries. This suggests that poor consolidation took place during sintering in spite of the fact that the final density was close to the theoretical density of the AA2124 alloy. On the contrary, SPS of MP (Fig. 9c and d) shows typical ductile failure manifested by the formation of dimples on the fractured surfaces of the consolidated Al-matrices surrounding encapsulated brittle oxide particles (pointed at by arrow).

On the other hand, SEM images of the NP consolidated and fractured surface shows that fracture occurred in between the particles, which indicates that the weakest points were in the inter-particle necks formed during sintering (Fig. 10). Once again this is due to the presence of the oxide films that encapsulate the nano particles and act as barriers to metal/metal diffusion during sintering. This was strongly manifested by the formation of microvoids (Fig. 10a and b pointed at by arrows) on the fracture surfaces of NP consolidate. It is suggested that the formed microvoids act as origins for microcrack propagation resulting in premature failure and hence the displayed lower ductility compared to the MP. At higher SEM magnifications of the fracture surface of the SPS NP (Figs. 11 and 12), whisker like particles growing perpendicular to the consolidated powder surface were observed. EDX analysis revealed that these whiskers were aluminum oxides with some Si content. One possible explanation for the formation of such whiskers is that they were formed post-sintering as SPS is known for its surface cleaning effect [18] which together with the residual porosities might have created a highly reactive surface. Ng et al. reported similar in situ formation of aluminum oxide whiskers or nano rods during low temperature sintering of aluminum-rich powder mixtures containing SiO_2, it was suggested that the presence of metal oxide particles is necessary for the oxidation of aluminum to form these whiskers/nanorods [19]. It is worth noting

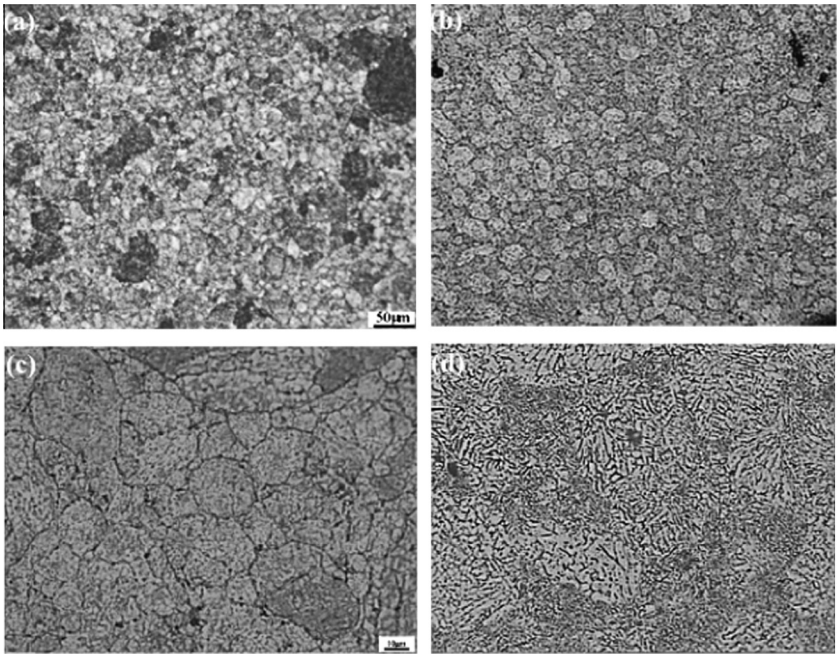

Fig. 5. Optical micrographs for MP specimens sintered with SPS (a, c) and HP (b, d).

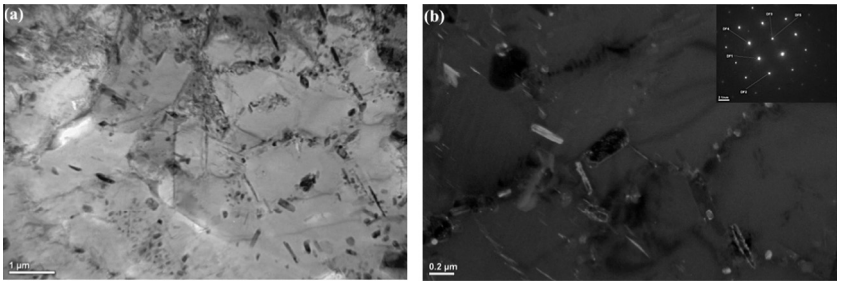

Fig. 6. TEM images of the MP specimens processed with SPS at different magnifications.

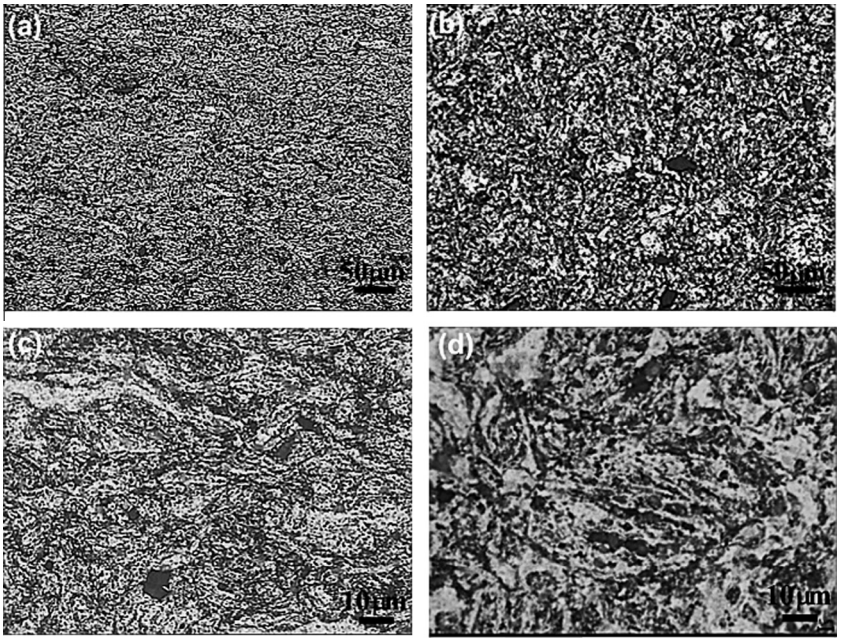

Fig. 7. Optical micrographs for NP specimens sintered with SPS (a, c) and HP (b, d).

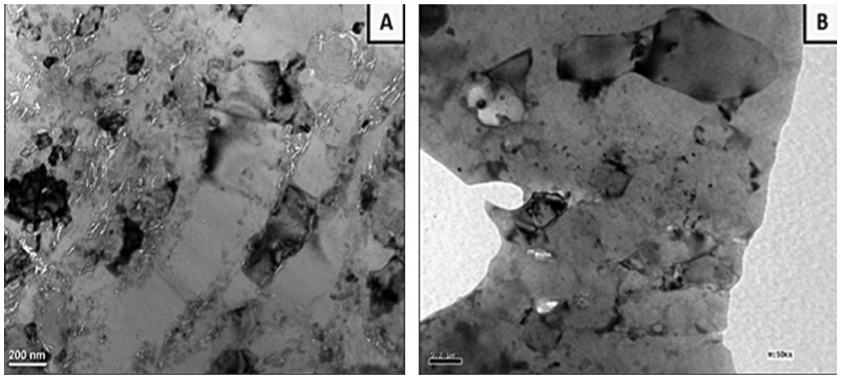

Fig. 8. TEM images for NP specimens sintered with SPS (a) and HP (b).

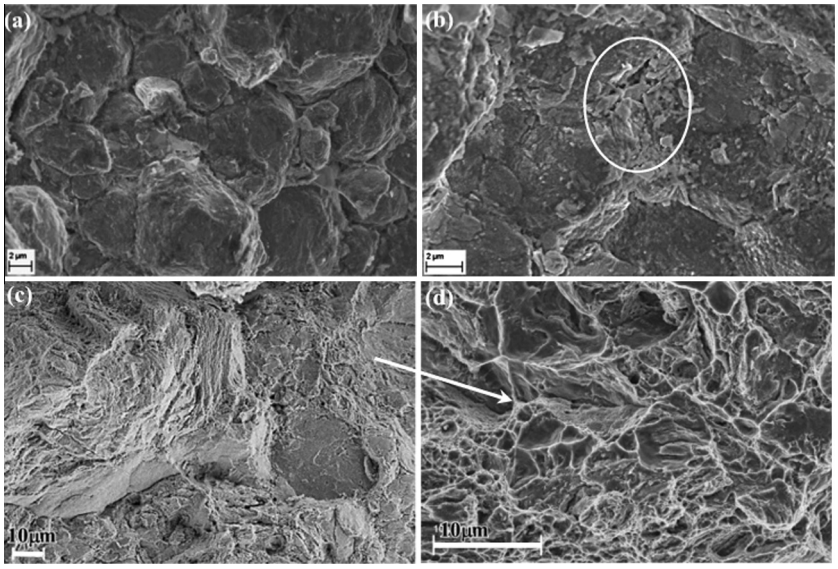

Fig. 9. Scanning electron micrographs of the fracture surface of the MP specimens processed with HP (a, b) and SPS (c, d) at low magnification and higher magnification, respectively.

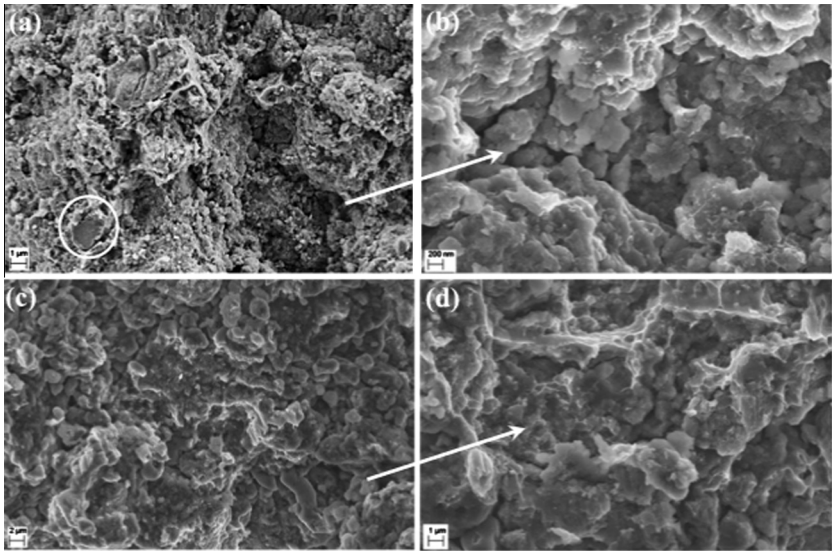

Fig. 10. Scanning electron micrographs of the fracture surface of the NP specimens processed with HP (a, b) and SPS (c, d) at low magnification and higher magnification.

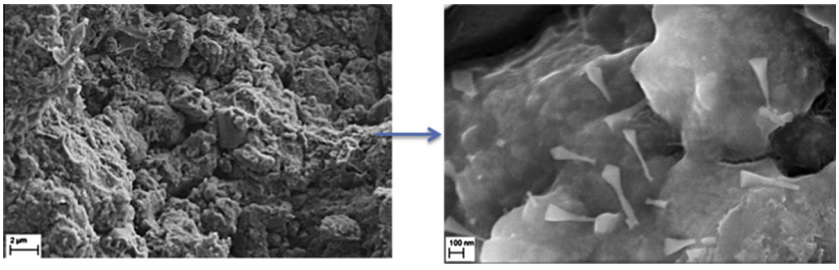

Fig. 11. High magnification SEM images showing oxide whisker formation in the spark plasma sintered NP structure.

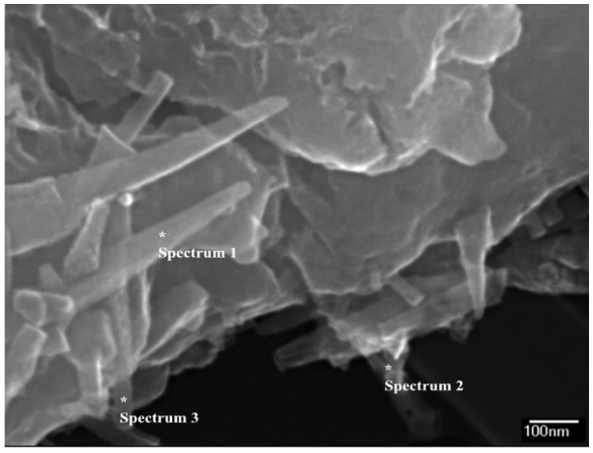

Processing option : All elements analyzed (Normalized)							
Spectrum	In stats.	O	Mg	Al	Si	Mn	Total
Spectrum 1	Yes	58.12	-0.57	39.98	2.27	0.2	100
Spectrum 2	Yes	63.86	0.58	34.03	1.71	-0.18	100
Spectrum 3	Yes	58.37	0.96	38.63	0.7	1.35	100

Fig. 12. SEM image of the aluminum oxide whiskers formed in the NP specimens processed through SPS and the corresponding EDX analysis data.

that the Oxide whiskers were not observed on the fracture surfaces of MP regardless of the sintering technique used.

4. Conclusions

The following conclusions can be drawn from this work:

1. Nano-crystalline bulk AA2124 (with AGS ~200 nm) was successfully produced after high energy ball milling for 36 h followed by SPS for 10 min at 480 °C.
2. Lower density levels were reached for the NP specimens after SPS and HP as a result of the presence of thin oxide films around the NP that are hard to break due to the increased dislocation density after ball milling.
3. Specimens produced via SPS showed enhanced mechanical properties when compared to their HP counterpart.
4. The NP specimens showed significant enhancement in hardness and compressive strength but lacked sufficient ductility due to the higher porosity levels and the presence of oxide dispersoids.
5. Optical microscopy showed that SPS specimens had a higher degree of uniform diffusion along the particle boundaries compared to HP specimens.
6. The NP specimens processed with SPS had a whisker like aluminum oxide phase that was formed after sintering; the mechanism of formation of this phase requires further investigations.

Acknowledgments

Authors of this work would like to acknowledge the Yousef Jameel Science and Technology Research Center at the American University in Cairo for the financial support and the facilitation of using the equipment necessary for characterization

References

[1] A.A. Karimpoor, U. Erb, K.T. Aust, G. Palumbo, Scripta Mater. 49 (2003) 651–656.
[2] S.R. Agnew, B.R. Elliott, C.J. Youngdahl, J.R. Weertman, Mater. Sci. Eng. A285 (2000) 391–396.
[3] L. Liu, Y. Li, F. Wang, J. Mater. Sci. Technol. 26 (1) (2010) 1–14.
[4] H.A. Padilla II, B.L. Boyce, Exp. Mech. 50 (2010) 5–23.
[5] Z.Q. Qi, J.C. Jiang, E.I. Meletis, Wear mechanism of nanocrystalline metals, in: 1st International Meeting on Developments in Materials, Process and Applications of Nanotechnology Belfast, North Ireland, pp. 4227–4232.
[6] C. Suryanarayana, Prog. Mater. Sci. 46 (2001) 1–184.
[7] A.A. Sadek and H.G. Salem, Construction of consolidation maps for pre-ECAE hot compact nanocrystalline-micron powders, in: Proceedings of the ASME 2nd Multifucntional Nanocomposites and Nanomaterials Conference and Exhibition (MN '08) Sharm El Sheikh, Egypt. CD-ROM, 2008, pp. 39–46.
[8] H.G. Salem, A.A. Sadek, J. Mater. Eng. Perform. 19 (3) (2010) 356–357.
[9] T.P. Rich, J.G. Orbison, R.S. Duncan, P.G. Olivero, R.H. Peterec, J. Mater. Eng. Perform. 8 (3) (1999) 315–324.
[10] Guang Rana, Jingén Zhou, Q.G. Wang, J. Alloys Comp. 421 (2006) 80–86.
[11] Mazher Ahmed Yar, Sverker Wahlberg, Hans Bergqvist, Hanadi G. Salem, Mats Johnsson, Mamoun Muhammed, Chemically produced nanostructured ods-lanthanum oxide–tungsten composites sintered by spark plasma sintering, J. Nucl. Mater. 408 (2) (2011) 129–135.
[12] Mazher Ahmed Yar, Sverker Wahlberg, Hans Bergqvist, Hanadi G. Salem, Mats Johnsson, J. Nucl. Mater. 412 (2) (2011) 227–232.
[13] J. Ye, L. Ajdelsztajn, J.M. Schoenung, Bulk nanocrystalline aluminum 5083 alloy fabricated by a novel technique: cryomilling and spark plasma sintering, Metall. Mater. Trans. 37A (2006) 2569–2679.
[14] J.K. Rana, D. Sivaprahasam, K.S. Raju, V.S. Sarma, Microstructure and mechanical properties of nanocrystalline high strength Al–Mg–Si (AA6061) alloy by high energy ball milling and spark plasma sintering, Mater. Sci. Eng. A527 (2009) 292–296.
[15] German, RM Sintering Theory and Practice, Wiley, New York NY, USA, 1996.
[16] G. Xie, O. Ohashi, T. Yoshioka, M. Song, K. Mitsuishi, H. Yasuda, K. Furuya, T. Noda, Mater. Trans. 42 (9) (2001) 1846–1849.
[17] C. Li-Hua, C. Yu-Yong, Z. Lai-Qu, L. Jun-Pin, Trans. Nonfer. Met. Soc. China. 22 (2012) 528–533.
[18] X. Song, X. Liu, J. Zhang, J. Am. Ceram. Soc. 89 (2) (2006) 494–500.
[19] Dickon H.L. Ng, P. Yu, N.G. Ma, C.K. Lo, W.Y. Kwok, M.Y. Yau, C.Y. To, T.K. Li, Cheng-Ji Deng, J. Eur. Ceram. Soc. 26 (2006) 1561–1565.